Fracture Toughness and Fatigue Crack Propagation Rate of Short Fiber Reinforced Epoxy Composites for Analogue Cortical Bone

Alexander C. M. Chong
Department of Mechanical Engineering,
University of Kansas,
Lawrence, KS 66045
e-mail: cmchong@ku.edu

Forrest Miller
Director of Engineering
e-mail: foss@pacific-research.com

McKee Buxton
Engineer
Pacific Research Laboratories, Inc.,
Vashon, WA 98070
e-mail: mckee@pacific-research.com

Elizabeth A. Friis[1]
Assistant Professor
Department of Mechanical Engineering,
University of Kansas,
Lawrence, KS 66045
e-mail: lfriis@ku.edu

Third-generation mechanical analogue bone models and synthetic analogue cortical bone materials manufactured by Pacific Research Laboratories, Inc. (PRL) are popular tools for use in mechanical testing of various orthopedic implants and biomaterials. A major issue with these models is that the current third-generation epoxy–short fiberglass based composite used as the cortical bone substitute is prone to crack formation and failure in fatigue or repeated quasistatic loading of the model. The purpose of the present study was to compare the tensile and fracture mechanics properties of the current baseline (established PRL "third-generation" E-glass–fiber–epoxy) composite analogue for cortical bone to a new composite material formulation proposed for use as an enhanced fourth-generation cortical bone analogue material. Standard tensile, plane strain fracture toughness, and fatigue crack propagation rate tests were performed on both the third- and fourth-generation composite material formulations using standard ASTM test techniques. Injection molding techniques were used to create random fiber orientation in all test specimens. Standard dog-bone style tensile specimens were tested to obtain ultimate tensile strength and stiffness. Compact tension fracture toughness specimens were utilized to determine plane strain fracture toughness values. Reduced thickness compact tension specimens were also used to determine fatigue crack propagation rate behavior for the two material groups. Literature values for the same parameters for human cortical bone were compared to results from the third- and fourth-generation cortical analogue bone materials. Tensile properties of the fourth-generation material were closer to that of average human cortical bone than the third-generation material. Fracture toughness was significantly increased by 48% in the fourth-generation composite as compared to the third-generation analogue bone. The threshold stress intensity to propagate the crack was much higher for the fourth-generation material than for the third-generation composite. Even at the higher stress intensity threshold, the fatigue crack propagation rate was significantly decreased in the fourth-generation composite compared to the third-generation composite. These results indicate that the bone analogue models made from the fourth-generation analogue cortical bone material may exhibit better performance in fracture and longer fatigue lives than similar models made of third-generation analogue cortical bone material. Further fatigue testing of the new composite material in clinically relevant use of bone models is still required for verification of these results. Biomechanical test models using the superior fourth-generation cortical analogue material are currently in development. [DOI: 10.1115/1.2746369]

Keywords: composite, cortical bone, fracture toughness, fatigue

1 Introduction

The use of mechanical analogue composite bone models in the evaluation of implants and surgical procedures has grown rapidly in recent years. The advantages of these composite analogue bones over cadaveric human bones include less interspecimen variability, ready availability, and ease of handling [1]. Additionally, composite bones do not deteriorate with time, making them possible bone substitutes for fatigue testing of surgical implant constructs in situ.

In 1987, Pacific Research Laboratories (PRL) introduced the first anatomically and structurally realistic mechanical analogue composite bone [2]. This first-generation analogue femur had a cortical bone analogue material consisting of epoxy reinforced with a braided tube of glass fiber. However, because of fiber sizing issues, this cortical bone analogue did not have adequate bonding between the glass fiber and epoxy (PRL, personal communication). In 1991, PRL introduced the second-generation of fiberglass–fabric-reinforced composite replicate bones. The second-generation composite bone was a combination of E-glass cloth, matt, and roving, layered around a rigid polyurethane foam core (which modeled the cancellous bone). E-glass is an alkali-free, alumino–borosilicate glass; E-glass fibers have excellent strength and are the most commonly used fiberglass. The cortical layer was formed by pressure injecting epoxy into the E-glass material that surrounded the foam core. Standard bone models

[1]Corresponding author.

Contributed by the Bioengineering Division of ASME for publication in the JOURNAL OF BIOMECHANICAL ENGINEERING. Manuscript received May 31, 2006; final manuscript received January 19, 2007. Review conducted by David Fyhrie. Paper presented at the 2005 ASME Summer Bioengineering Conference.

were manufactured with a solid rigid polyurethane foam cancellous core material, that is, without an open intramedullary canal, unless cellular rigid polyurethane foam was specified by the customer [2].

The second-generation composite fiberglass laminate bone models required manual craftsmanship. These models were thus less than ideal in terms of ease of manufacture, anatomic detail, and reproducibility of mechanical properties, both within and between specimens [3]. Though these second-generation bones did reproduce the general strain pattern generated on the surface of the fresh frozen human cadaveric femur under simulated physiological loading, because of their highly anisotropic layout, they did not allow investigators to easily section the bones to reproduce surgical procedures used in implantation techniques (PRL, personal communication). For these reasons, PRL introduced the third-generation composite analogue bone models that utilized short-glass-fiber-reinforced (SGFR) epoxy for the cortical analogue material. The third-generation bones modeled natural cortical bone using a mixture of short E-glass fibers and epoxy resin pressure-injected around a polyurethane foam core. Third-generation composite bone was developed to improve the composite bone physical behavior, increase reproduction of anatomic detail in the cortical wall, and ease manufacturing difficulties associated with the second-generation bone models [2]. In addition, the SGFR analogue cortical bone was more uniform and isotropic; it gave investigators the ability to saw and broach the models easily to better replicate orthopedic surgical procedures.

Third-generation composite cortical bone has been used in a variety of bone models [2]. The femur and tibia models made with third-generation composite cortical bone have been validated for rigidity in comparison to human cadaveric bones [3]. Third-generation composite femurs were used to study the effects of resting periods, which are a considerable part of the daily activity cycle on the migration characteristics of cemented femoral stems [4]. Because of the increased ease in manufacturing, other anatomically accurate analogue bones have been made from the third-generation composite material; for example, analogue vertebrae used in mechanical analogue spine models [5] have been produced, but not yet validated. Many investigators have used these third-generation bones in clinically based hypothesis-driven research projects. For example, the third-generation femur models were used to study the effect of bone cement mixing technique on subsidence of Exeter polished hip implants [6]. Anatomically accurate analogue lumbar spine models utilizing analogue composite soft tissues and third-generation bone mechanical analogue vertebrae have been used with implanted pedicle screws to estimate the effect of fusion level on facet joint load and intervertebral disc pressure [5].

Common to many of these studies is the problem of early crack formation or fatigue failure of the composite analogue cortical bone [4–6]. Figure 1 illustrates crack formation on the lateral side of a third-generation composite femur at the location of the distal tip of a cemented femoral implant. These cracks typically formed at the site of stress concentration at the distal tip of the implant after 2–3 million cycles of mulated one-legged stance loading [6,7]. Such damage forms at the distal implant tip in vivo in hip replacement patients, but is normally presented as midthigh pain and can heal by bone buildup remodeling or calcification before complete structural failure of the implant-bone construct occurs [8–11]. Markolf and Amstutz found a large scatter in fatigue life in implanted cadaveric femurs, most likely due to variations in bone quality, geometry, surgical technique, and implant positioning [7]. For the type of implant used in their study, they speculated that a load of up to one-fourth the ultimate of the cadaveric femur in one-legged loading stance could be applied without fatigue failure of the construct. The value of three times average body weight typically applied for simulated one-legged stance is above the value of one-fourth of average ultimate load for cadaveric femurs, thus indicating that cadaveric femurs would not be suitable for use in fatigue studies. A synthetic femur model that can withstand cyclic loading and be comparable with the fatigue performance of the self-repairing human bone is needed [6,7,12].

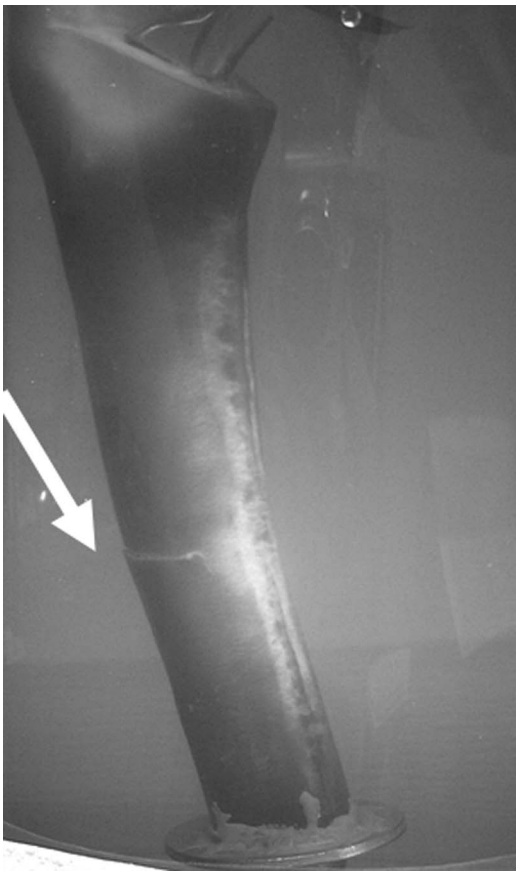

Fig. 1 Third-generation femur implanted with a cemented femoral stem that had been fatigue loaded in single legged stance [6]. The arrow points to the location of the early crack formation in the third-generation analogue bone material; cracks formed due to stress concentrations at the tip of the implant and low fatigue resistance of the third-generation material.

Similarly, pedicle screws used in spine fusion procedures can generate local remodeling in vertebra. Composite vertebrae have been made using third-generation composite analogue cortical bone materials, but unlike bone of living human vertebrae, the composite cortical bone materials cannot remodel. As shown in Fig. 2, with repeated loading the bone around pedicle screws in analogue vertebrae has been shown to occasionally form fatigue cracks and fracture in ways that do not replicate the clinical scenario [5]. These examples demonstrate the need for improvement of the fatigue and fracture properties of the third-generation composite cortical bone analogue material. In order to address these issues, PRL developed a proprietary formulation fourth-generation composite cortical bone analogue material that may have enhanced resistance to fracture and fatigue.

The present study is the first research to characterize the tensile, fracture, and fatigue properties of the third- and fourth-generation PRL composite analogue cortical bones. The overall objective of determining if the fatigue performance of the fourth-generation materials was superior to the performance of the third-generation materials. The major portion of the fatigue life of a material may be taken up in the propagation of a crack. Through application of linear elastic fracture mechanics principles, it is possible to predict the number of cycles spent in growing a crack to some specified length or to final failure. Fatigue crack propagation rate tests,

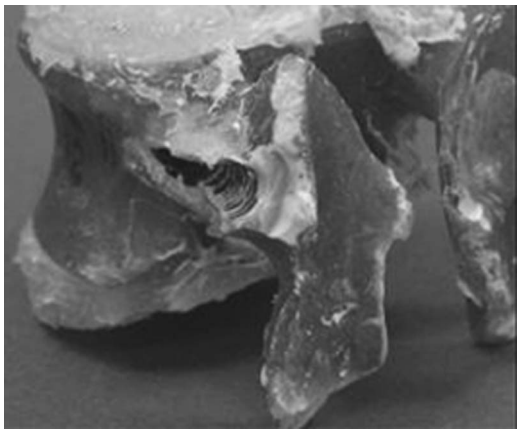

Fig. 2 Composite analogue vertebrae made from third-generation experience fracture after use in testing with pedicle screws. Fatigue cracks developed in the analogue vertebrae around the pedicle screw insertion sites.

though perhaps not as pleasing in the interpretation of results as extensive fatigue limit tests, are often used to compare fatigue performance of materials. If done in combination with tensile strength and fracture toughness analysis, the fatigue crack propagation rate analysis gives insight into the fatigue resistance of various materials without performing the much more time consuming and expensive full fatigue characterization. Therefore, the three specific objectives of this study were to determine if: (1) the static mechanical properties of the fourth-generation analogue cortical bone material were similar to those for human cortical bone; (2) the fracture toughness of the fourth-generation composite was greater than the third-generation material and in the range of literature values for human cortical bone; and (3) the fatigue crack propagation resistance of the fourth-generation bone analogue materials was greater than that for the third-generation materials.

Standard tensile, fracture toughness, and fatigue crack propagation rate test methods were performed on both material combinations. The third-generation composite analogue bone was considered as the base line for comparison and literature data was used to compare to properties for human cortical bone. It was hypothesized that the static mechanical properties and fracture toughness of the fourth-generation bone analogue would be in the range of reported literature data for human cortical bone and greater than that for the third-generation materials. The fatigue crack propagation rate tests were used to compare and help predict if the fourth-generation composite material would exhibit longer lifetimes under fatigue loading when used in a bone model. Though the details are proprietary, the fourth-generation materials were selected by the manufacturer in an attempt to increase resistance to fatigue loading. Therefore, it was hypothesized that the fourth-generation materials would exhibit greater resistance to fatigue crack propagation than the third-generation composite cortical bone analogue.

2 Methods

The study consists of three experimental parts: equilibrium tensile testing for material properties, Mode I plane strain fracture toughness (K_{Ic}) experiments, and fatigue crack propagation rate (FCPR) experiments. All tests were performed under precisely defined procedures dictated by the American Society for Testing and Materials (ASTM) D638-03 (tensile test), E1820-01 (K_{Ic} test), and E647-00 (FCPR test) standards [13–16].

2.1 Materials. The materials evaluated in this investigation were two commercially available SGFR epoxy polymer composites designated as "third-generation E" and the new "fourth-generation" analogue cortical bone material, as dictated by the bone analogue manufacturer (PRL, Vashon, WA). The exact type and amount of fiber, fiber surface treatment, fiber length, resin, and hardener used in these materials are proprietary. For both materials in all specimen types, the composite mixture was injection molded into and cured in molds in a manner similar to that used in making analogue bone models. As a result, the short fibers in both the third- and the fourth-generation analogue materials were randomly oriented in all specimen types. Both materials were therefore assumed to have isotropic apparent mechanical properties.

2.2 Tensile Testing. The third-generation and fourth-generation synthetic analogue bone materials were tested in accordance with ASTM D638-03 [16]. Injection-molded standard dog-bone specimens of 152.4 mm length, and 3.2 mm thickness were loaded to failure in tension at room temperature in the ambient air environment on a screw-type mechanical test system (Instron 4204) at a displacement rate of 2.54 mm/s (6 in./min). A

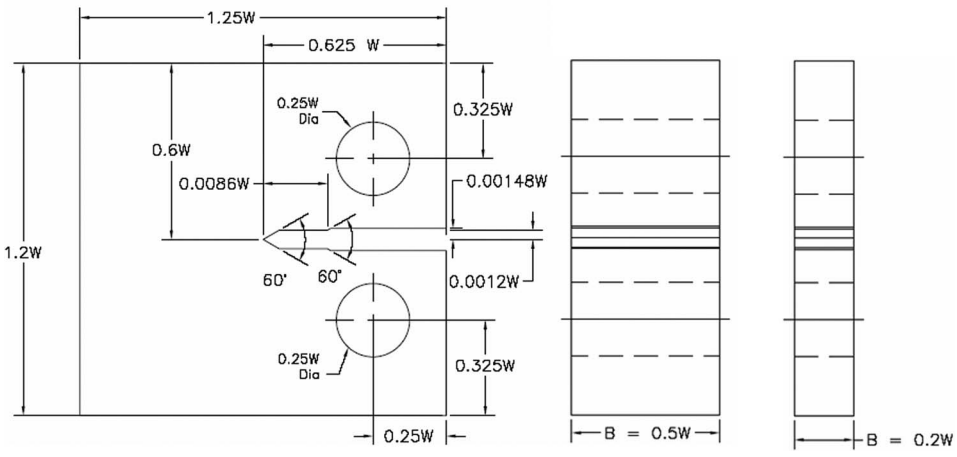

Fig. 3 Dimensioned drawing of the standard single edge-notched compact specimen for K_{Ic} and FCPR testing, based on ASTM E1820-01 and E647-00 standards [13,14]. (*a*) Detailed dimensions of the compact test specimen for both K_{IC} and FCPR test specimen; (*b*) dimensions for the K_{Ic} test specimen thickness; and (*c*) dimensions for the FCPR test specimen thickness. The specimen width, W=63.50 mm (2.5 in.), was determined based on the above mentioned ASTM standards.

50.8 mm extensometer was mounted on the gauge section on each specimen, and load and extensometer data were recorded to failure. Five specimens of each material type were tested. Ultimate tensile strength and elastic modulus were determined using ASTM dictated procedures. Average property values and standard deviations for each material type were determined and single factor analysis of variance (ANOVA) was used for statistical comparison of the results between the third- and fourth-generation composites. Only percent differences were used to compare results of the composite material testing results to literature values of human cortical bone properties reported in the literature, as there were substantial differences in specimen sizes between studies.

2.3 Fracture Toughness (K_{Ic}) Tests. Fracture toughness tests were performed on both the third- and fourth-generation analogue cortical bone materials according to ASTM E1820-01. The compact tension [$C(T)$] specimen shape was selected. To ensure plane strain conditions, it was first necessary to determine the specimen size required.

2.3.1 Fracture Toughness Specimen Size Determination. The initial selection of $C(T)$ specimen size for the K_{Ic} tests was made by using the method employing the ratio of yield strength to Young's modulus. Since no previous fracture toughness data were available, the material yield strength was assumed to be equal to the tensile strength and subsequently used in estimating the required specimen size. The average ratio of tensile strength to Young's modulus of the third- and fourth-generation composites was calculated to be 0.007, therefore the conservative minimum required specimen thickness, B, was determined to be 31.75 mm [13]. The crack length, a, of the $C(T)$ standard specimen which is equal to the crack starter notch plus fatigue crack, must be nominally equal to the thickness, B, and must be between 0.45 and 0.55 times the width, W. The ratio of width to thickness, must be at least two, therefore, the required specimen width, W, was determined to be 63.50 mm [13]. This conservative estimate of required specimen size helped to ensure that the plane strain fracture toughness values determined for these two materials were valid and reproducible. Schematic diagrams of the ASTM standard $C(T)$ K_{Ic} test specimen used are shown in Figs. 3(a) and 3(b) [13,15].

2.3.2 Fracture Toughness Test Methods. Blocks of the materials tested were injection molded with the required thickness. Each block was cut and machined to yield four fracture toughness specimens. Initial notches, as shown in Fig. 3(a) were machined into each specimen, thus ensuring random fiber orientation at the notch tip. All K_{Ic} test specimens were tested under tension-tension axial loading with all data measured and collected by the servo-hydraulic mechanical test system (MTS Model 858, Mini Bionix II, Eden Prairie, MN). Figure 4 shows a photograph of the experimental K_{Ic} setup in the test system. The testing setup included with a 25 kN load cell, axial actuator with 100 mm stroke, two tension-testing clevis jigs, two adaptors, two lock pins, a test specimen, and a light source for crack visualization during testing.

Each construct was first subjected to specimen fatigue precracking produced by cyclically loading the specimen in tension with preselected minimum and maximum loads at 8 Hz under displacement control, with an approximate load ratio of $R=0.1$ maintained by periodically changing displacement ranges. The maximum load, as dictated in the standard procedures, was approximately 90% of the measured ultimate load for the specimen until the final required fatigue precrack length between 0.45 W and 0.55 W was achieved [13]. Once the crack length reached the minimum precrack length, red spray paint was applied to the crack space while the specimen was under load. Red spray paint was applied to the cracked specimen before final fracture so that the physical precrack length before fracture could be identified on the fractured specimen surfaces. The visible physical fracture precrack length is a critical parameter that must be measured at various locations through the specimen thickness in order to determine plane strain fracture toughness.

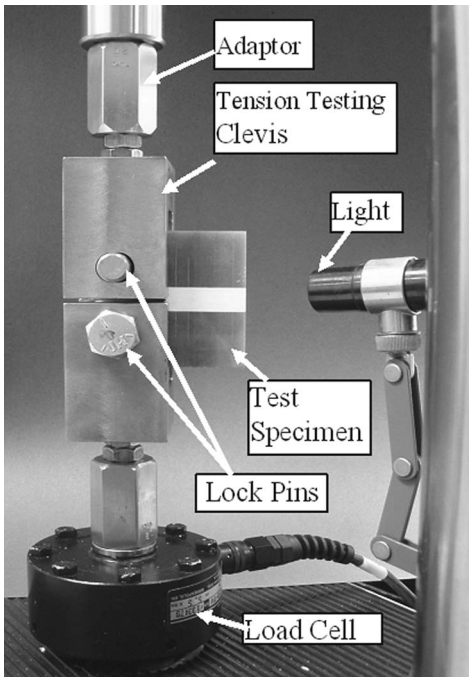

Fig. 4 Photograph of the K_{Ic} experimental setup. Note that a thin layer of whiteout on the surface of the test specimen was for crack visualization; the whiteout had no effect on the composite material. The light source was also used for crack visualization during testing.

Once the paint dried, the specimen was loaded at a constant displacement rate of 0.02 mm/s until complete fracture. During each run, load and displacement readings were recorded using the MTS Mini Bionix II data collection system at a data acquisition frequency of 25 Hz. Digital pictures were taken of the top and bottom pieces of the broken specimen and used to measure the physical fracture crack length profile, as indicated by the region of dried red paint. The standard test method dictates a minimum required percent uniformity of the precrack length across the thickness of the specimen as well as a minimum average precrack length. Particularly in composite materials, variations in precrack length across the thickness are common, so often tested specimen results must be rejected. Only data from specimens that met the precrack length uniformity criteria were considered valid and used in further analysis. Initial groups of 12 specimens were tested for each material type with increments of four specimens added to achieve a minimum number of eight valid specimens per material type.

K_Q is the provisional fracture toughness value calculated until the K_Q value can be shown to have been measured under plane strain test conditions [13]. If this condition is shown, then K_Q is equal to K_{Ic}. The provisional plane strain fracture toughness K_Q of a material for the compact specimen is determined as shown in Eqs. (1) and (2)

$$K_Q = \left(\frac{P_Q}{B^*\sqrt{W}}\right) * f\left(\frac{a}{W}\right) \tag{1}$$

where

$$f\left(\frac{a}{W}\right)=\frac{\left(2+\frac{a}{W}\right)*\left(0.886+4.64^{*}\frac{a}{W}-13.32^{*}\left(\frac{a}{W}\right)^{2}+14.72^{*}\left(\frac{a}{W}\right)^{3}-5.6^{*}\left(\frac{a}{W}\right)^{4}\right)}{\left(1-\frac{a}{W}\right)^{3/2}} \tag{2}$$

and a is the crack length; B is the specimen thickness; W is the specimen width; and P_Q is the qualified load required to break the specimen defined as the intersection of 95% slope with load-displacement curve [13].

In order for the K_Q calculation to be validated as the valid K_{Ic} value, two conditions shown in Eqs. (3) and (4) must be satisfied

$$2.5^{*}(K_Q/\sigma_{YS})^2 \leq B \tag{3}$$

and

$$P_{\max}/P_Q \leq 1.10 \tag{4}$$

where $P_{\max}$ is the overall maximum load [13]. Not meeting the requirements of Eq. (3) would indicate that the test was done under substantially mixed plane strain and plane stress conditions and that the K_Q value would not be a constant material property. If the relationship in Eq. (4) is not upheld, the required conditions for application of linear elastic fracture mechanics theory does not apply and the test method is invalid. If one or both of these two parameters in Eqs. (3) and (4) are not achieved, the test is not a valid K_{Ic} test. Once validity of plane strain results were verified, the student's t-tests and single factor ANOVA were performed to compare K_{Ic} results between the two sample groups. Only percent differences were used to compare results of the composite fracture toughness values to literature values of human cortical bone properties reported in the literature, as there were substantial differences in specimen sizes and shapes between studies.

2.4 Fatigue Crack Propagation Rate Tests. Fatigue crack propagation rate tests were performed on both the third- and fourth-generation analogue cortical bone materials according to ASTM E647-00. The $C(T)$ specimen shape was again selected, with size changes required as compared to the fracture toughness tests.

2.4.1 FCPR Specimen Size Determination. Standard test methods employed recommend that the thickness of the FCPR specimen, B_2, must be within the range $W/20 \leq B_2 \leq W/4$. Specimen width, W, from K_{Ic} testing was determined to be 63.5 mm, therefore, the acceptable range of B_2 becomes $3.175 \leq B_2 \leq 15.875$ mm. The specimen width was selected to be 12.7 mm. Schematic diagrams of the ASTM standard $C(T)$ FCPR test specimen are shown in Figs. 3(a) and 3(c) [13,14].

2.4.2 FCPR Test Methods. Fatigue crack propagation rate experiments were performed according to ASTM E647-00 [14] Crack propagation gauges (Vishay Measurements Group, Raleigh, NC) were mounted with the first gauge wire located 4 mm in front of the machined notch. As the crack progressed into the specimen, strands of the gauge wire fractured at the crack location. Electrical resistance of the gauge was then altered, thus showing a change in voltage corresponding to a given crack length. Circuitry was developed to link the output of the crack propagation gauges with number of cycles into a computer data acquisition system. In this manner, the number of cycles and crack length at a given time and number of loading cycles were simultaneously obtained. During each run, the crack propagation gauge signal readings were amplified by a factor of 800 and then acquired through the data acquisition card in the MTS Mini Bionix II test system.

Eight specimens of each material type were tested. Each specimen construct was first subjected to fatigue precracking produced by using the MTS Mini Bionix servohydraulic test system and test jigs from the fracture toughness testing with centralizing spacers to account for the reduction in thickness. Cyclic tensile loading was applied with preselected minimum and maximum loads (90% of the estimated ultimate load) at 8 Hz under load control with load ratio of 0.1. Standards dictate a fatigue precrack length of at least 0.25 mm [14]. Once the precrack length was achieved, the frequency was reduced to 5 Hz with the same applied load range. Changes in crack length, a, and number of cycles, N, were recorded continuously until the fatigue crack propagated through the entire gauge thickness to complete failure of the specimen. Using this data, the secant or point-to-point technique was used to calculate crack growth rate, da/dN, for each crack extension range by determining the slope of the straight line connecting two adjacent data points on the crack length, a, versus number of cycles, N, curve. The stress intensity threshold, ΔK, needed to initiate crack formation was calculated by the ASTM dictated relationships given in Eqs. (5) and (6), where B and W are the previously defined specimen thickness and width, and ΔP was the difference between the applied minimum and maximum loads [14]

$$\Delta K=\frac{\Delta P(2+\alpha)}{B\sqrt{W}(1-\alpha)^{3/2}}(0.886+4.64\alpha-13.32\alpha^2+14.72\alpha^3-5.6\alpha^4) \tag{5}$$

where

$$\alpha=\frac{a}{W} \tag{6}$$

The fatigue crack growth response can be divided into three main regions: initiation, propagation, and termination. For comparing materials, the primary interest was only in Region II, propagation, and in the stress intensity threshold, ΔK, needed to initiate crack formation. In Region II, the power law usually models crack propagation behavior according to the equation

$$\frac{da}{dN}=C(\Delta K)^n \tag{7}$$

where n and C are constants for a given material [14]. The slope of the log ΔK versus log da/dN in Region II is the material parameter, n, that can be used in combination with stress intensity threshold, ΔK, to compare the fatigue crack propagation rate potential of the two materials. In accordance with standard techniques, data for all specimens tested for each material type were plotted on one log ΔK versus log da/dN graph [14]. The secondary linear Region II on this data plot was determined according to standard definitions, and the average slope of the region calculated for both the third-generation and fourth-generation cortical bone analogue composites [14]. Average values of n and ΔK were compared and percent differences determined, but due to the nature of these analyses, more advanced statistical calculations were not possible.

3 Results and Discussion

Table 1 lists the results of the tensile tests on the third- and fourth-generation composite cortical bone analogue materials. The fourth-generation composite showed statistically significant increases of 37% ($p=0.004$) in tensile strength and 39% ($p<0.001$) in elastic modulus as compared to the third-generation material. Values of tensile strength and elastic modulus for human

Table 1 Average tensile strength and tensile modulus test results for the third- and fourth-generation analogue cortical bone materials as compared to values for human cortical bone in both the longitudinal and transverse directions [17]

	Ultimate tensile strength		Tensile elastic modulus	
Bone material	(MPa)	Percent difference from third generation (%)	(GPa)	Percent increase from third generation (%)
Third generation ($n=5$)	78±5.3	—	11.3±0.6	—
Fourth generation ($n=5$)	107±5.8	37 ($p=0.004$)	15.8±0.2	39 ($p<0.001$)
Human cortical, longitudinal ($n=35$)[a]	132±16.1	—	17.7±3.9	—
Human cortical, transverse ($n=21$)[a]	57.9±5.5	—	13.1±3.1	—

[a]See Refs. [17,18].

cortical bone as reported in the literature are also given in Table 1 [17]. The ultimate tensile strength and tensile modulus of fresh frozen human cortical bone in the longitudinal direction has been reported to be 131.8 MPa and 17.3 GPa, respectively [17,18]. Cortical bone is highly anisotropic; strength and stiffness of fresh frozen human cortical bone in the transverse direction has been reported to be 57.9 MPa and 13.1 GPa, respectively [17,18]. Substantial variation for both parameters was found for differences in age, quality, direction, and location [17]. The average ultimate tensile strength and tensile elastic modulus of the fourth-generation material were found to be 107 MPa and 16 GPa, respectively, compared to values of 78 MPa and 11 GPa for tensile strength and tensile modulus, respectively, of third-generation material. The tensile strength and tensile modulus of the fourth-generation analogue cortical bone are much closer to the average values of human cortical bone than the third-generation analogue bone [17,18]. These results indicate that the fourth-generation cortical analogue material has tensile properties that are closer to simple averages of the longitudinal and transverse reported tensile properties of human cortical bone (94.9 MPa strength and 15.4 GPa stiffness), as compared to the third-generation material. Statistical comparison of the third- and fourth-generation materials to values reported for human cortical bone would not be appropriate, as the tensile specimen size and shape was much smaller for the human bone samples [17,18]. These literature values, however, do provide a range of comparison for the synthetic analogue cortical bone materials.

Both the third- and fourth-generation composite analogue bone materials were tested and analyzed for Mode I plane strain fracture toughness (K_{Ic}). Table 2 lists the number of specimens of both material types tested, the number of specimens that yielded valid test results according to uniformity requirements in crack length across the thickness [13], the resulting average and standard deviation of K_Q measured from valid tests, and the percent increase from the third-generation material baseline. A total of eight third-generation specimens (out of 12 tested) and nine fourth-generation specimens (out of 20 tested) were found to have suitable uniform precrack lengths. K_Q test results were verified to be valid K_{Ic} values for all tests. The average fracture toughness of the fourth-generation material was significantly higher ($p<0.001$) than the third-generation by an average of 48%. In a recent review of the literature, Wang and Puram reported data of fracture toughness values obtained by several investigators [19]. Values of fracture toughness for human compact cortical bone using compact tension specimens have been reported to range from 1.6 MPa $m^{1/2}$ to 8.3 MPa $m^{1/2}$, depending on the location of the bone, direction, and quality [19]. Both the third- and fourth-generation analogue cortical bone materials had plane strain fracture toughness values within this range, though the fourth-generation fracture toughness was closer to the average values shown in the literature for human cortical bone in the longitudinal direction [19]. It is recognized that all these tests used linear elastic fracture mechanics relationships, but that because of the source limitations on sizes of bone specimens that can be used, true plane strain dominant specimen size conditions imposed by ASTM E1820 may not have been met [20]. A small specimen size can allow plane stress conditions to influence the fracture toughness measured and yield values that are higher than if plane strain dominant conditions were maintained. The specimen size used in these tests was not identical to that used in this study; these literature values, however, do provide a range of comparison for the synthetic analogue cortical bone materials.

Third-generation and fourth-generation analogue cortical bone materials were tested to measure their FCPR behavior. Figure 5 illustrates representative da/dN versus ΔK data on a log-log scale to compare the overall results of the fatigue propagation rate for both materials. The average power relationship in Region II (the intermediate region) for third- and fourth-generation materials within the bound of their scatter data is given in Eqs. (8) and (9), respectively [14]

Table 2 Summary of fracture toughness (K_{Ic}) test results for the third- and fourth-generation synthetic analogue cortical bone material. Valid specimens must meet ASTM guidelines in terms of crack shape and length. The initial fracture toughness parameter, K_Q, was shown to be equal to K_{Ic} for all valid specimens tested. The range of literature values measured for human cortical bone are also listed for comparison [19].

Bone material	Number of specimens tested	Number of valid specimens	K_{Ic} (MPa $m^{1/2}$)	Percent increase from third generation (%)
Third generation	12	8	2.76±0.27	—
Fourth generation	20	9	4.07±0.31	48 ($p<0.001$)
Human cortical bone[b]	—	—	1.6–8.3	—

[b]See Ref. [19].

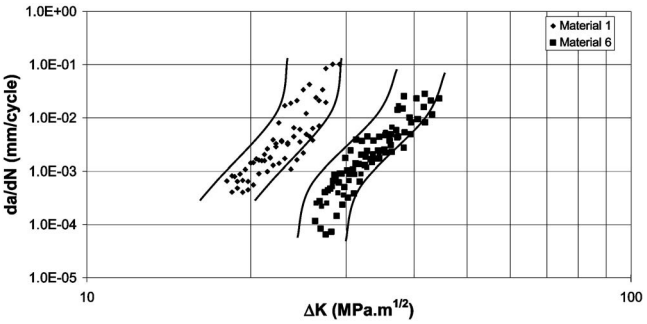

Fig. 5 Log-log scale graphical presentation of *da/dN* versus ΔK fatigue crack propagation pooled specimen results for the third- and fourth-generation bone analogue materials. The lines drawn on the graph are the boundaries of the fatigue crack growth response regimes [14].

$$(da/dN)_{3\text{rd Gen}} = 3 \times 10^{-11}(\Delta K)^{5.855} \tag{8}$$

and

$$(da/dN)_{4\text{th Gen}} = 2 \times 10^{-10}(\Delta K)^{4.588} \tag{9}$$

When individual specimen behavior was compared, the average slope of the propagation region of the fourth-generation material was significantly lower than for third-generation material by 31% ($p=0.004$). As can be seen from these data, the fourth-generation material has improved fatigue crack propagation resistance even at high ΔK levels. At lower ΔK levels, there is a significant difference in fatigue crack propagation behavior for the two composite materials. It is also noteworthy that there were considerable differences in threshold ΔK_{th} for the two materials. ΔK_{th} is defined as the fracture crack propagation threshold below which crack propagation would not occur; in another words, when $\Delta K < \Delta K_{th}$, $da/dN=0$. A greater stress intensity was required to initiate cracking in the fourth-generation than in the third-generation material. When comparing FCPR behavior two similar materials, it is typically desirable to maintain the same stress intensity threshold level so that the value of "*n*" can be better interpreted and compared. This was not possible for the two materials tested, as the ΔK required for the fourth-generation material was so much greater than for the third-generation materials. Had the ΔK required for the fourth-generation materials been used on the third-generation materials, the specimens would have broken at nearly first loading. This result is logical because the fourth-generation material demonstrated significantly higher fracture toughness than the third-generation material. All these parameters indicate that the fourth-generation material is likely to have a higher fatigue life than the third-generation material. For use in biomechanical test models, a higher fatigue life is always desirable, as synthetic materials cannot heal themselves as live bone does in vivo.

4 Conclusion

Tensile properties, plane strain fracture toughness, and fatigue crack propagation behavior of the PRL third- and fourth-generation composite analogue cortical bone materials were characterized. For each property, the fourth-generation material demonstrated mechanical properties that were closer to reported properties for fresh frozen human cortical bone than the third-generation material [17–19]. The fourth-generation material also showed a higher threshold ΔK_{th} and fatigue crack propagation resistance compared to the third-generation material. For these reasons, it is expected that the fatigue resistance of the fourth-generation cortical analogue material should be superior and provide better performance of biomechanical test models (such as the analogue femur) for use in repeated quasistatic and fatigue studies. Further studies on in situ fatigue testing of the bone models with the fourth-generation materials in comparison to the third-generation materials are recommended. Previous studies have shown problems in excessive model subsidence in the third-generation bone models [6]. Though it is not expected, testing of fourth-generation models will reveal if they also demonstrate similar types of inappropriate behaviors that cannot be predicted by the tests done in this study. In addition, it is possible that temperature and environment may influence the fatigue behaviors of the composite analogue materials; further work in analysis fatigue behavior in a clinically relevant environment is also recommended.

Acknowledgment

The authors are grateful to Mr. Matt Hess for his technical assistance and Pacific Research Laboratories, Inc. for providing the materials to do this work.

References

[1] Cristofolini, L., Viceconti, M., and Cappello, A., 1996, "Mechanical Validation of Whole Bone Composite Femur Models," J. Biomech., **29**(4), pp. 525–535.
[2] Sawbones® Worldwide 2005, Pacific Research Laboratories, Inc., Vashon, WA, https://secure.sawbones.com/products/bio/composite.asp.
[3] Heiner, A. D., and Brown, T. D., 2001, "Structure Properties of a New Design of Composite Replicate Femurs and Tibias," J. Biomech., **34**, pp. 773–781.
[4] Verdonschot, N., Barink, M., Stolk, J., Gardeniers, J. W. M., and Schreurs, B. W., 2002, "Do Unloading Periods Affect Migration Characteristics of Cemented Femoral Components? An In Vitro Evaluation With the Exeter Stem," Acta Orthop. Belg., **68**, pp. 348–355.
[5] Friis, E. A., Pence, C. D., Graber, C. D., and Montoya, J. A., 2002, Mechanical Analogue Model of the Human Lumbar Spine: Development and Initial Evaluation, Spinal Implants: Are We Evaluating Them Appropriately?, *ASTM STP 143*, M. N. Melkerson, S. L. Griffith, and J. S. Kirkpatrick, eds., ASTM International, West Conshohocken, PA, pp. 143–154.
[6] Whitaker, C., Czuwala, P. J., McQueen, D. A., Cooke, F. W., and Friis, E. A., 2003, "Subsidence Rate of Polished Femoral Prostheses: Effect of Bone Cement Porosity," American Academy of Orthopedic Surgeons, New Orleans, LA, Poster No. P063.
[7] Oh, I., and Harris, W. H., 1978, "Proximal Strain Distribution in the Loaded Femur. An In Vitro Comparison of the Distributions in the Intact Femur and After Insertion of Different Hip-Replacement Femoral Components," J. Bone Jt. Surg., Am. Vol., **60**(1), pp. 75–85.
[8] Bergh, M. S., Muir, P., Markel, M. D., and Manley, P. A., 2004, "Femoral Bone Adaptation to Stable Long-Term Cemented Total Hip Arthroplasty in Dogs," Vet. Surg., **33**(3), pp. 214–220.
[9] Brown, T. E., Larson, B., Shen, F., and Moskal, J. T., 2002, "Thigh Pain after Cementless Total Hip Arthroplasty: Evaluation and Management," J. Am. Acad. Orthop. Surg., **10**(6), pp. 385–392.
[10] Draenert, K. D., Draenert, Y. I., Krauspe, R., and Bettin, D., 2005, "Strain Adaptive Bone Remodeling in Total Joint Replacement," Clin. Orthop. Relat. Res., **430**, pp. 12–27.
[11] Lavernia, C., D'Apuzzo, M., Hernanadez, V., and Lee, D., 2004, "Thigh Pain in Primary Total Hip Arthroplasty: The Effect of Elastic Moduli," J. Arthroplasty, **19**(7/2), pp. 10–16.
[12] Markolf, K. L., and Amstutz, H. C., 1980, "Mechanical Strength of the Femur Following Resurfacing and Conventional Total Hip Replacement Procedures," Clin. Orthop. Relat. Res., **147**, pp. 170–180.
[13] ASTM, 2001, "Standard Test Method for Measurement of Fracture Toughness," *Annual Book of ASTM Standards, 03.01, Specification E1820-01*, West Conshohocken, PA, pp. 1031–1076.
[14] ASTM, 2001, "Standard Test Method for Measurement of Fatigue Crack Growth Rates," *Annual Book of ASTM Standards, 03.01, Specification E647-00*, West Conshohocken, PA, pp. 603–644.
[15] ASTM, 2001, "Standard Test Method for Plane-Strain Fracture Toughness of Metallic Material," *Annual Book of ASTM Standards, 03.01, Specification E399-90(1997)*, West Conshohocken, PA, pp. 443–473.
[16] ASTM, 2005, "Standard Test Method for Tensile Properties of Plastics," *Annual Book of ASTM Standards, 08.01, Specification D638-03*, West Conshohocken, PA, pp. 47–61.
[17] Burstein, A. H., Reilly, D. T., and Martens, M., 1976, "Aging of Bone Tissue: Mechanical Properties," J. Bone Jt. Surg., Am. Vol., **58**(1), pp. 82–86.
[18] Reilly, D. T., and Burstein, A. H., 1975, "The Elastic and Ultimate Properties of Compact Bone Tissue," J. Biomech., **8**(6), pp. 393–405.
[19] Wang, X., and Puram, S., 2004, "The Toughness of Cortical Bone and its Relationship with Age," Ann. Biomed. Eng., **32**(1), pp. 123–135.
[20] Yang, Q. D., Cox, B. N., Nalla, R. K., and Ritchie, R. O., 2006, "Re-evaluating the Toughness of Human Cortical Bone," Bone (N.Y.), **38**(6), pp. 878–887.